

Article

An ultra-low loss CaMgGeO₄ microwave dielectric ceramic and its chemical compatibility with silver electrodes for LTCC applications

Huaicheng Xiang, Chunchun Li, Heli Jantunen, Liang Fang, and Arthur Hill

ACS Sustainable Chem. Eng., Just Accepted Manuscript • DOI: 10.1021/
acssuschemeng.8b00220 • Publication Date (Web): 26 Mar 2018

Downloaded from <http://pubs.acs.org> on March 26, 2018

Just Accepted

"Just Accepted" manuscripts have been peer-reviewed and accepted for publication. They are posted online prior to technical editing, formatting for publication and author proofing. The American Chemical Society provides "Just Accepted" as a service to the research community to expedite the dissemination of scientific material as soon as possible after acceptance. "Just Accepted" manuscripts appear in full in PDF format accompanied by an HTML abstract. "Just Accepted" manuscripts have been fully peer reviewed, but should not be considered the official version of record. They are citable by the Digital Object Identifier (DOI®). "Just Accepted" is an optional service offered to authors. Therefore, the "Just Accepted" Web site may not include all articles that will be published in the journal. After a manuscript is technically edited and formatted, it will be removed from the "Just Accepted" Web site and published as an ASAP article. Note that technical editing may introduce minor changes to the manuscript text and/or graphics which could affect content, and all legal disclaimers and ethical guidelines that apply to the journal pertain. ACS cannot be held responsible for errors or consequences arising from the use of information contained in these "Just Accepted" manuscripts.

An ultra-low loss CaMgGeO_4 microwave dielectric ceramic and its chemical compatibility with silver electrodes for LTCC applications

Huaicheng Xiang^{1,2}, Chunchun Li^{1,3*}, Heli Jantunen², Liang Fang^{1*}, Arthur E. Hill⁴

¹*State Key Laboratory Breeding Base of Nonferrous metals and specific Materials Processing,
Guangxi universities key laboratory of non-ferrous metal oxide electronic functional materials
and devices, College of Materials Science and Engineering, Guilin University of Technology,
541004, Guilin, China*

²*Microelectronics Research Unit, Faculty of Information Technology and Electrical Engineering,
University of Oulu, FI-90014 Oulu, Finland*

³*College of Information Science and Engineering, Guilin University of Technology, 541004,
Guilin, China*

⁴*Materials and Physics Research Centre, School of Computing, Science & Engineering, University
of Salford, The Crescent, Salford, M5 4WT, UK*

* Corresponding Author, lichunchun2003@126.com (C. Li); fanglianggl001@aliyun.com (L. Fang).

xianghuaicheng@126.com (H. Xiang), Guilin University of Technology, 541004, Guilin, China.

lichunchun2003@126.com (C. Li), Guilin University of Technology, 541004, Guilin, China.

Heli.Jantunen@oulu.fi (H. Jantunen), University of Oulu, 4500, FI-90014 Oulu, Finland.

fanglianggl001@aliyun.com (L. Fang), Guilin University of Technology, 541004, Guilin, China.

a.e.hill@salford.ac.uk (A.E. Hill), University of Salford, The Crescent, Salford, M5 4WT, UK.

ABSTRACT

A new ultra-low dielectric loss co-fired CaMgGeO_4 dielectric material with olivine structure was fabricated by the solid-state route. The X-ray patterns, Rietveld refinement, and microstructure revealed the characteristics of the synthesized material. CaMgGeO_4 ceramic belongs to the orthorhombic system with a $Pbmn$ space group. Sintered at 1300 °C for 6 h, the ceramic exhibited a densification of 96.5 %, an ultra-high quality factor ($Q \times f$) of 124,900 GHz ($\tan \delta = 1.24 \times 10^{-4}$) at a frequency of 15.5 GHz, a permittivity (ϵ_r) of 6.71, and a temperature coefficient of resonant frequency (τ_f) of -73.7 ppm/°C and the average CTE of CaMgGeO_4 was 12.4 ppm/°C. The sintering temperature of the CaMgGeO_4 ceramic could be reduced from 1300 to 940 °C with the addition of 5wt% B_2O_3 . The $\text{CaMgGeO}_4 + 5\text{wt}\% \text{B}_2\text{O}_3$ ceramics exhibited favorable microwave dielectric performances: $Q \times f = 102,000$ GHz (at 16.4 GHz), $\epsilon_r = 5.80$, and $\tau_f = -64.7$ ppm/°C, respectively. In addition, the CaMgGeO_4 ceramic did not react with Ag electrodes, which could be advantageous in LTCC multilayer microwave devices.

KEYWORDS: Microwave dielectric properties, CaMgGeO_4 , LTCC, ultra-low dielectric loss.

INTRODUCTION

The recent rapid advance in wireless communication systems has encouraged the spread of dielectric materials into diverse applications such as dielectric resonators, filters, substrates, capacitors, oscillators, etc.^{1,2} These applications require microwave dielectrics with a low dielectric loss ($\tan\delta = 1/Q$, $Q \times f$: quality factor, f : resonant frequency in microwave region) to achieve a high selectivity and durability in microwave components, a low permittivity (ϵ_r) to diminish the signal transmission time, and a temperature coefficient of resonant frequency (τ_f) close to zero for the stability of the electronic devices in different temperature environments.³⁻⁵ In addition, miniaturization is the required development trend of such materials in order for them to be incorporated into integrated circuits. The miniaturization can be realized by using low-temperature co-fired ceramic (LTCC) technology because LTCC technology can stack ceramics and inner electrodes into a multilayer structure to achieve the required thickness.⁶ Silver is usually used as a metal electrode layer due to its high conductivity. Therefore, microwave dielectric ceramics need to be developed to enable LTCC devices with a lower melting point than that of the Ag electrodes (960 °C).⁷⁻⁹ The traditional method to drop the temperature of ceramics is to add sintering aids, such as glasses or low melting point oxides, although this usually results in the deterioration of the $Q \times f$ values.^{10,11} Recent investigations have suggested that B₂O₃ could dramatically decrease the sintering temperature of ceramics without significantly degrading their performance because B₂O₃ is easy to evaporate at high temperatures over 900 °C.^{12,13}

Germanates with an olivine structure (space group *Pbmn*) with the general formulas Me_2GeO_4 (Me = Mg, Zn, Ca, Ba) have attracted much interest due to their thermal, mechanical, pyroelectric, and dielectric properties.¹⁴⁻¹⁶ For example, Zn_2GeO_4 has promising dielectric properties at 1300 °C ($\epsilon_r = 6.87$, $Q \times f = 102,700$ GHz, $\tau_f = -32.4$ ppm/°C),¹⁷ and Mg_2GeO_4 sintered at 1250 °C has a low $\epsilon_r = 5.48$, a $\tau_f = -27.61$ ppm/°C, and a $Q \times f = 11,037$ GHz.¹⁸ Nevertheless, the sintering temperature of the above ceramics is too high to co-fire with metallic electrodes or for application in LTCC multilayer devices. In 1995 van Duijn et al.¹⁹ first reported the formation and structure of CaMgGeO_4 , which belongs to the olivine structure with a general formula $\text{A}_2^{2+}\text{B}^{4+}\text{O}_4^{2-}$, but the performances of CaMgGeO_4 ceramics at microwave region have not previously been investigated. Here, we report the ultra-low dielectric loss of CaMgGeO_4 ceramic with olivine structure, the method of synthesis, densification process, and microwave dielectric properties. In addition, the influence of B_2O_3 as a sintering aid on the density, sinterability, and microwave dielectric properties of CaMgGeO_4 is also examined.

EXPERIMENTAL SECTION

CaMgGeO_4 ceramic specimens were fabricated via the solid-state reaction of high-purity oxides (>99%) CaO, MgO, and GeO_2 . The raw oxides were ball-milled for 6 h using absolute ethanol ($\text{CH}_3\text{CH}_2\text{OH}$, $\geq 99.7\%$) as an intermediary and the wet oxides were dried at 120 °C. Two-step sintering at 900 °C and 1250 °C for 6 h were employed to obtain CaMgGeO_4 . The CaMgGeO_4 system has a sequence of chemical reaction:

$$\text{CaCO}_3 + \text{MgO} + \text{GeO}_2 \xrightarrow{900^\circ\text{C}} \text{CaO} + \text{MgO} + \text{GeO}_2 + \text{CO}_2 \uparrow \xrightarrow{1250^\circ\text{C}}$$

CaMgGeO₄. The fired powders were milled secondly for 6 hours. The powders were compressed into green disks with 10 mm×5 mm (diameter × thickness) for microwave dielectric measurements mixed with polyvinyl alcohol (5 wt.%) as the binder at a pressure of 200 MPa. The disks were first sintered at 550 °C to burn out the PVA (temperature rate of 1.5 °C/min) and further sintered at 1260-1340 °C with a temperature rate of 5 °C/min.

The crystal structure and phase purity of CaMgGeO₄ were analyzed by X-ray diffractometer (X'Pert PRO, Netherlands). The Rietveld analysis was performed on the XRD pattern using the FullProf program. The microstructure images were studied by scanning electron microscopy (JSM6380-LV, Japan) and the Archimedes principle was used to measure the density of ceramics. The ϵ_r , $Q \times f$, and τ_f were measured at microwave frequency by a vector network analyzer (10 MHz-40 GHz, N5230A, Agilent, USA) and an oven (9039, USA) in the temperature range of 25-85 °C. The τ_f was calculated by Equation (1):

$$\tau_f = \frac{f_2 - f_1}{f_1(T_2 - T_1)} \quad (1)$$

In the equation, f_1 and f_2 denote the resonant frequencies at temperatures T_1 (25 °C) and T_2 (85 °C). The linear coefficient of thermal expansion (CTE) of the CaMgGeO₄ ceramic was estimated utilizing Thermal Dilatometer (DIL402C, NETZSCH, Germany).

RESULTS AND DISCUSSION

Figure 1(a) gives the XRD pattern of the CaMgGeO₄ sample calcined at 1250 °C for 6 hours. The XRD peaks of the sample matched with the standard JCPDS PDF No.36-1483 and the calcined specimen was a single phase with olivine structure in space group *Pbmn*. The refined cell parameters were $a = 11.2491(1) \text{ \AA}$, $b = 6.4018(6) \text{ \AA}$, $c = 4.9977(7) \text{ \AA}$, and $V = 359.9151(0) \text{ \AA}^3$. All atomic coordinates are listed in Table I and the crystal structure of the CaMgGeO₄ sample is depicted in the inset of Figure 1(b). The Mg occupies a symmetrical center. Ca and Mg occupying factors indicated a complete ordering of these two atoms. There are three different oxygen atoms, and the Ca atoms are connected to four O(1), one O(2), and one O(3). The Mg atoms are connected to two O(1), two O(2), and two O(3). The Ge atoms are coordinated by two O(1), one O(2), and one O(3). This structure is composed of [MgO₆] octahedra sharing edges with each other to form a chain parallel to [001]. The bands are connected by [CaO₆] octahedrons and share edges with them. Separate [GeO₄] tetrahedrons help to connect the chains in the (100) plane.¹⁹

The Raman spectrum of CaMgGeO₄ between 60 and 1050 cm⁻¹ is depicted in Figure 2. 36 Raman-active vibration modes ($11A_g + 7B_{1g} + 11B_{2g} + 7B_{3g}$) were calculated for the olivine structure with the *Pbmn* symmetry according to the group theory. However, only 12 Raman active modes were fitted, which is much lower than the calculated ones because of peak overlapping.²⁰ The modes below 200 cm⁻¹ (B_{2g}) were assigned to the lattice vibrations caused by cation ions. In B_{1g} , clear modes were found at 216 cm⁻¹, 371 cm⁻¹, and 383 cm⁻¹, and the modes 284 cm⁻¹, 431 cm⁻¹ and 475 cm⁻¹ were assigned as B_{3g} . The high-frequency modes at 650-800 cm⁻¹ (A_g)

correspond to the stretching modes of the $[\text{GeO}_4]$ tetrahedron.

The SEM pictures recorded on the surfaces of the CaMgGeO_4 ceramics sintered at various temperatures are shown in Figure 3. When sintered from 1260 to 1280 °C, the sample presented a moderately dense microstructure with some pores, as shown in Figure 3(a) and (b). At 1300 °C, the porosity decreased, a dense uniform microstructure was observed and the grain boundaries were clear, as shown in Figure 3(c). However, following further increases of the temperature, it was obvious that grains of abnormal growth and pores were formed, as shown in Figure 3(d) and (e). This was probably due to the excessive sintering temperatures.

Figure 4 exhibits the change of density, ϵ_r , $Q \times f$ and τ_f values of CaMgGeO_4 ceramics with the sintering temperature. As the sintering temperature increased the relative density gradually increased to the highest value $\sim 3.57 \text{ g/cm}^3$ at 1300 °C. The theoretical density of the CaMgGeO_4 ceramic is 3.70 g/cm^3 and so the maximal relative density could reach 96.5 % at 1300 °C. The decrease of density at temperatures over 1300 °C may be due to over-heating and heterogeneous exaggerated grain growth. This was consistent with the changes seen in the SEM images.

As shown in Figure 4(b), the ϵ_r first increased, reached a peak value of 6.71 at 1300 °C and then reduced with rising temperature. Generally, the permittivity at microwave frequencies relies on the densities, any secondary phases, and ionic polarizability, etc.^{20,21} In the present work, the effects of second phases and density on

the ε_r value may be negligible because the XRD analysis did not detect the second phases and the CaMgGeO_4 ceramic possessed a high density. The theoretical permittivity can be explained by the total of individual ionic polarizability and the molar volume of a compound in accordance with Clausius-Mossotti equation:^{22,23}

$$\varepsilon_{th} = \frac{3V + 8\pi\alpha}{3V - 4\pi\alpha} \quad (2)$$

In the equation, V is the cell volume and α is the molecular polarizability. The total of ionic polarizability of CaMgGeO_4 could be derived from the equation:

$$\alpha(\text{CaMgGeO}_4) = \alpha(\text{Ca}^{2+}) + \alpha(\text{Mg}^{2+}) + \alpha(\text{Ge}^{4+}) + 4\alpha(\text{O}^{2-}) \quad (3)$$

where $\alpha(\text{Ca}^{2+})$, $\alpha(\text{Mg}^{2+})$, $\alpha(\text{Ge}^{4+})$, and $\alpha(\text{O}^{2-})$ are 3.16 \AA^3 , 1.32 \AA^3 , 1.63 \AA^3 and 2.01 \AA^3 , respectively. The ε_{th} of CaMgGeO_4 is 6.79, which is extremely close to the measured value. The relative error between ε_r and ε_{th} for CaMgGeO_4 is 1.17 %, which implies that there is no other mechanism of polarization in the microwave frequency band for CaMgGeO_4 ceramic.²⁴

Figure 4(c) demonstrates the relationship between $Q \times f$ values and temperature of CaMgGeO_4 ceramics. It was observed that the change in the $Q \times f$ values was similar to the apparent densities with temperature. These variations were considered to relate to the densifications, and the high $Q \times f$ value usually corresponds to the high densification.^{25,26} At the best densification temperature of 1300°C , the CaMgGeO_4 ceramic exhibited an ultra-high $Q \times f$ value of $124,900 \text{ GHz}$ (corresponding to an ultra-low dielectric loss of 1.24×10^{-4}) at a frequency of 15.5 GHz . Normally, the

factors influencing the dielectric loss could be divided into two major classes: the internal factors largely relying on inharmonic terms in the crystal potential energy, and the external factors correlated to the grain boundaries, density, lattice defects, impurities, etc. Kim *et al.*²⁷ summarized that the packing fraction of a structure is a key factor affecting $Q \times f$. They showed that a rise in packing fraction can reduce the lattice vibrations, producing an increase in the quality factor. In the crystal structure, each ion is considered as a rigid sphere. The ratio of the volume of ions at each site to the total unit cell volume is an effective packing fraction. For CaMgGeO₄ ceramic, the packing fraction may be determined by the equation (4):

$$\begin{aligned} \text{packing fraction (\%)} &= \frac{\text{volume of packed ions}}{\text{volume of unit cell}} \times Z \\ &= \frac{4\pi/3 \times (r_{Ca}^3 + r_{Mg}^3 + r_{Ge}^3 + 4 \times r_O^3)}{V} \times 4 \end{aligned} \quad (4)$$

In the equation, r is the ionic radius. The calculated packing fraction of CaMgGeO₄ ceramic was 57.76 %.

Within the sintered range of 1260-1340 °C, the τ_f values of CaMgGeO₄ ceramic experienced only small changes and remained steady at about -74 ppm/°C (Figure 4(d)). The τ_f values were affected by the temperature coefficient of relative permittivity (τ_ϵ) and the linear thermal expansion coefficient (α_L), as the equation (5):²⁸

$$\tau_f = -\left(\frac{\tau_\epsilon}{2} + \alpha_L\right) \quad (5)$$

Because the α_L of microwave dielectric ceramic is about 10 ppm/°C,²⁹ the τ_ϵ value

would play a primary role in CaMgGeO₄ ceramic. Using Equation (2), Bosman and Havinga inferred the formula of τ_ε .^{30,31}

$$\tau_\varepsilon = \frac{1}{\varepsilon} \left(\frac{\partial \varepsilon}{\partial T} \right) = \frac{(\varepsilon - 1)(\varepsilon + 2)}{3\varepsilon} (A + B + C) \quad (6)$$

$$\begin{aligned} A &= \frac{1}{\alpha_m} \left(\frac{\partial \alpha_m}{\partial T} \right)_V \\ B &= \frac{1}{\alpha_m} \left(\frac{\partial \alpha_m}{\partial V} \right)_T \left(\frac{\partial V}{\partial T} \right)_P \\ C &= -\frac{1}{V} \left(\frac{\partial V}{\partial T} \right)_P \end{aligned} \quad (7)$$

where ε , α_m , and A describe the relative permittivity, polarizability, and direct dependence of the polarizability on temperature, respectively. A is generally negative. The term B is positive and C is negative, and they are also very similar in magnitude. Hence, in CaMgGeO₄ ceramic, a positive ($A+B+C$) value corresponded to a negative τ_f value. Figure 5 shows the CTE curve of CaMgGeO₄ sintered at 1300 °C. The inset of Figure 5 gives the change of CTE with different temperatures and the average CTE of CaMgGeO₄ is 12.4 ppm/°C.

In consideration of the close correlation between τ_f and τ_ε values, it is meaningful to determine the τ_ε value of CaMgGeO₄ for practical applications and for a further understanding of the τ_f value. Figure 6 shows the temperature dependence of ε_r and $\tan\delta$ at four different frequencies (1 kHz, 10 kHz, 100 kHz, and 1 MHz). As seen, in the lower temperature area (from room temperature to 250 °C), both ε_r and $\tan\delta$ exhibited only slight variation with increasing temperature, indicating their temperature stability in this temperature region. However, a remarkable increase in

both values with obvious frequency dispersion was observed, which might be due to the increase in conductivity with increasing temperature. The inset of Figure 6 shows the enlarged profile at 25-250 °C measured at 1 MHz, from which τ_e was calculated to be 149 ppm/°C. According to equation (5), the calculated τ_f value was -86.9 ppm/°C which was close but a little higher than the measured value, ~ -73.7 ppm/°C for CaMgGeO₄. Notably, the relative permittivity measured at 1 MHz was about 9.15, which was much higher than the value (6.71) measured at microwave frequency. This indicates that in the RF region another polarizability mechanism contributes to the permittivity.

To further lower the densification temperature of the CaMgGeO₄ to below 960 °C, various amounts of B₂O₃ were added to the CaMgGeO₄ samples. The choice of B₂O₃ was guided by previous successful applications in lowering the sintering temperature of several materials^{32,33}. In the current work 1, 3, 5, and 7 wt.% B₂O₃ were used to determine the optimum doping content. The bulk densities of CaMgGeO₄ + x wt.% B₂O₃ ($x = 1, 3, 5$, and 7) as a function of sintering temperature are depicted in Figure 7. As observed, B₂O₃ doping effectively reduced the densification temperature of CaMgGeO₄ ceramic to 1220 °C at 1 wt.% B₂O₃ and to 940 °C at 5 wt.% B₂O₃, and further to 920 °C at 7 wt.% B₂O₃, which was much lower than the temperature of pure CaMgGeO₄ ceramic (1300 °C). At lower dosages, ≤ 5 wt.% B₂O₃ addition did not reduce the bulk density of CaMgGeO₄ with a highest density of 3.62 g/cm³ in CaMgGeO₄ + 5 wt.% B₂O₃ sintered at 940 °C. However, 7 wt.% B₂O₃ resulted in an apparent decrease in bulk density, which was due to the

appearance of secondary phases, as approved by XRD analysis. Figure 8 gives the XRD patterns of CaMgGeO₄ ceramic with different B₂O₃ additions sintered at their relative densification temperatures for 6 h. By indexing with the JCPDF card, it was clearly observed that the XRD pattern of 1 wt.% B₂O₃-added CaMgGeO₄ was very alike to that of the single ceramic but when the B₂O₃ content increased to 3 wt.% and 5 wt.%, an additional peak attributed to an unknown second phase was detected. However, at $x = 7$, B₂O₃ (JCPDS NO. 24-0160) and Ca₃B₂O₆ (JCPDS NO.26-0885) secondary phases were formed along with the major CaMgGeO₄ phase, suggesting a chemical reaction between CaMgGeO₄ and B₂O₃. The lower bulk densities of B₂O₃ and Ca₃B₂O₆ (2.46 g/cm³ and 3.11 g/cm³, respectively) could explain the relatively low bulk density of CaMgGeO₄ + 7 wt.% B₂O₃. These results indicate that appropriate amount B₂O₃ addition can dramatically reduce the sintering temperature of CaMgGeO₄ whereas high-level doping reduces the formation of second phases which would degrade the dielectric performances. Thus, 5 wt.% B₂O₃ was selected as the optimum dosage to reduce the sintering temperature of CaMgGeO₄.

The microwave dielectric properties, density, and sintering temperature of CaMgGeO₄ + 5wt% B₂O₃ ceramics are listed in Table II. The 5 wt.% B₂O₃ added into CaMgGeO₄ ceramic could dramatically reduce the sintering temperature from 1300 to 940 °C, and the material exhibited good microwave dielectric characteristics: $Q \times f = 102,000$ GHz (at 16.4 GHz), $\epsilon_r = 5.80$ and $\tau_f = -64.7$ ppm/°C. Compared with the parent CaMgGeO₄ ceramic, B₂O₃ addition induced a slight degradation in the $Q \times f$ and ϵ_r . As is well-known, the dielectric properties in the microwave frequency region

are sensitive to the influence of extrinsic factors, especially any second phase(s).^{34,35}

Therefore, the decrease in dielectric performance of the B₂O₃-added samples could be partly explained by the appearance of the second phase which was detected by the XRD analysis.

For LTCC multilayer microwave device applications the chemical compatibility of CaMgGeO₄ ceramic with silver electrodes should be evaluated. Therefore, a mixture of 5wt% B₂O₃ added CaMgGeO₄ ceramic powder with 20 wt.% Ag powder was co-fired and examined to identify any potential reactions between them. The XRD patterns, BSE image and EDS analysis of CaMgGeO₄ + 5 wt.% B₂O₃ + 20 wt.% Ag samples co-fired at 940 °C for 6h are presented in Figure 9. Only diffraction peaks of CaMgGeO₄ and Ag were detected in the XRD patterns. Additionally, the BSE image showed two different kinds of grains with clear boundaries. EDS analysis indicated that the smaller grains included the elements Ca, Mg, Ge and O, and the ratio of Ca:Mg:Ge was nearly 1:1:1. Thus the smaller grains should be the CaMgGeO₄ phase, and the larger grains was Ag. The reason for the larger size of the Ag grains compared to the CaMgGeO₄ ceramic grains might be associated with the difference in the temperature of sintering between pure Ag and CaMgGeO₄ ceramic. Pure silver has a lower sintering temperature, thus when sintered at the same temperature the silver grains could grow faster, leading to the observed larger Ag grains. All the above results imply that CaMgGeO₄ ceramic could be a possibility for applications in LTCC multilayer microwave devices.

Table III gives the dielectric performances of some ultra-low loss dielectric

materials. In contrast, $Q \times f$ of the present CaMgGeO_4 ceramic is comparable to willemite, forsterites, rock-salt compounds, and the complex perovskite $\text{Ba}(\text{Zn}_{1/3}\text{Ta}_{2/3})\text{O}_3$ (BZT), but it is much lower than the complex perovskite $\text{Ba}(\text{Mg}_{1/3}\text{Ta}_{2/3})\text{O}_3$ (BMT). It is well known that prolonging heat treatment over 100 hours is essential for BMT and BZT ceramics to achieve good dielectric properties, but this would increase energy consumption in fabrication. Thus, the simple processing, low sintering temperature, and desirable dielectric performances make CaMgGeO_4 -based materials important supplements for the LTCC multilayer device.

CONCLUSION

A novel ultra-low dielectric loss co-fired CaMgGeO_4 microwave dielectric material was fabricated by the solid phase sintering route. The XRD and Rietveld refinement indicated that CaMgGeO_4 ceramic belonged to the orthorhombic system with a $Pbmn$ space group. The ceramic sintered at 1300 °C/6 h exhibited a density of 96.5 % and an average CTE of 12.4 ppm/°C. The CaMgGeO_4 ceramic possessed excellent microwave properties: $Q \times f = 124,900$ GHz ($\tan \delta = 1.24 \times 10^{-4}$, $f = 15.5$ GHz), $\epsilon_r = 6.71$, and $\tau_f = -73.7$ ppm/°C. The densification temperature of CaMgGeO_4 ceramic could be reduced from 1300 to 940 °C when 5wt% B_2O_3 was added. $\text{CaMgGeO}_4 + 5\text{wt}\% \text{B}_2\text{O}_3$ ceramics also exhibited good microwave dielectric properties with $Q \times f = 102,000$ GHz (at 16.4 GHz), $\epsilon_r = 5.80$, and $\tau_f = -64.7$ ppm/°C. In addition, the chemical compatibility of CaMgGeO_4 with Ag electrodes opens up its application in LTCC technology.

1
2
3
4
5
6
7
8
9
10
11
12
13
14
15
16
17
18
19
20
21
22
23
24
25
26
27
28
29
30
31
32
33
34
35
36
37
38
39
40
41
42
43
44
45
46
47
48
49
50
51
52
53
54
55
56
57
58
59
60

ACKNOWLEDGMENTS

We appreciate the financial support from Natural Science Foundation of China (Nos. 51502047, 21561008, and 21761008), Project of Scientific Research and Technical Exploitation Program of Guilin (2016010702-2 and 20170225), and Natural Science Foundation of Guangxi Zhuang Autonomous Region (Nos. 2015GXNSFFA139003, 2016GXNSFBA380134, and 2016GXNSFAA380018). Author H. Xiang gratefully acknowledges the Graduate School of Guilin University of Technology.

REFERENCES

1. Sebastian, M. T.; Ubic, R.; Jantunen, H. Low-loss dielectric ceramic materials and their properties. *Int. Mater. Rev.* **2015**, *60*, 392–412, DOI 10.1179/1743280415Y.0000000007.
2. George, S.; Sebastian, M. T. Synthesis and microwave dielectric properties of novel temperature stable high Q, $\text{Li}_2\text{ATi}_3\text{O}_8$ (A = Mg, Zn) ceramics. *J. Am. Ceram. Soc.* **2010**, *93*, 2164–2166, DOI 10.1111/j.1551-2916.2010.03703.x.
3. Li, C. C; Xiang, H. C; Xu, M. Y.; Khaliq, J.; Chen, J. Q.; Fang, L. Low-firing and temperature stable microwave dielectric ceramics: $\text{Ba}_2\text{LnV}_3\text{O}_{11}$ (Ln = Nd, Sm). *J. Am. Ceram. Soc.* **2018**, *101* (2), 773–781, DOI 10.1111/jace.15251.
4. Varghese, J.; Siponkoski, T.; Teirikangas, M.; Sebastian, M. T.; Uusimäki, A.; Jantunen, H. Structural, dielectric, and thermal properties of Pb free molybdate based ultralow temperature glass. *ACS Sustainable Chem. Eng.* **2016**, *4*, 3897–3904, DOI 10.1021/acssuschemeng.6b00721.
5. Zhou, D.; Pang, L. X.; Wang, D. W.; Li, C.; Jin, B.; Reaney, I. M. High permittivity, low loss microwave dielectrics suitable for 5G resonator and low temperature co-fired ceramic architecture. *J. Mater. Chem. C* **2017**, *5*, 10094–10098, DOI 10.1039/C7TC03623J.
6. Joseph, N.; Varghese, J.; Siponkoski, T.; Teirikangas, M.; Sebastian, M. T.; Jantunen, H. Glass-free CuMoO_4 ceramic with excellent dielectric and thermal properties for ultralow temperature cofired ceramic applications. *ACS*

- Sustainable Chem. Eng.* **2016**, *4*, 5632–5639, DOI 10.1021/acssuschemeng.6b01537.
7. Guo, J.; Zhou, D.; Wang, H.; Yao, X. Microwave dielectric properties of $(1-x)\text{ZnMoO}_4\text{-}x\text{TiO}_2$ composite ceramics. *J. Alloys Compd.* **2011**, *509*, 5863–5865, DOI 10.1016/j.jallcom.2011.02.155.
8. Abhilash, P.; Sebastian, M. T.; Surendran, K.P. Glass free, non-aqueous LTCC tapes of $\text{Bi}_4(\text{SiO}_4)_3$ with high solid loading. *J. Eur. Ceram. Soc.* **2015**, *35*, 2313–2320, DOI 10.1016/j.jeurceramsoc.2015.02.002.
9. Zhou, D.; Li, J.; Pang, L. X.; Wang, D. W.; Reaney, I. M. Novel water insoluble and sustainable $(\text{Na}_x\text{Ag}_{2-x})\text{MoO}_4 (0 \leq x \leq 2)$ microwave dielectric ceramics with spinel structure sintered at 410 degrees. *J. Mater. Chem. C* **2017**, *5*, 6086–6091, DOI 10.1039/C7TC01718A.
10. Li, C. C.; Xiang, H. C.; Xu, M. Y.; Tang, Y.; Fang, L. Li_2AGeO_4 (A = Zn, Mg): Two novel low-permittivity microwave dielectric ceramics with olivine structure. *J. Eur. Ceram. Soc.* **2018**, *38*, 1524–1528, DOI 10.1016/j.jeurceramsoc.2017.12.038.
11. Wu, J. M.; Huang, H. L. Effect of crystallization on microwave dielectric properties of stoichiometric cordierite glasses containing B_2O_3 and P_2O_5 . *J. Mater. Res.* **2000**, *15*, 222–227, DOI 10.1557/JMR.2000.0036.
12. Fang, L.; Tang, Y.; Chu, D. J.; Zhou, H. F.; Zhang, H.; Chen, X. L.; Liu, Q. W. Effect of B_2O_3 addition on the microstructure and microwave dielectric

- properties of $\text{Li}_2\text{CoTi}_3\text{O}_8$ ceramics. *J. Mater. Sci. Mater. Electron.* **2012**, *23*, 478–483, DOI 10.1007/s10854-011-0421-y.
13. Wu, S. P.; Luo, J. H.; Cao, S. X. Microwave dielectric properties of B_2O_3 -doped ZnTiO_3 ceramics made with sol–gel technique. *J. Alloys Compd.* **2010**, *502*, 147–152, DOI 10.1016/j.jallcom.2010.04.131.
14. Koseva, I.; Nikolov, V.; Petrova, N.; Tzvetkov, P.; Marychev, M. Thermal behavior of germanates with olivine structure. *Thermochim. Acta* **2016**, *646*, 1–7, DOI 10.1016/j.tca.2016.11.004.
15. Nagai, T.; Asai, S.; Okazaki, R.; Terasaki, I.; Taniguchi, H. Effects of element substitution on the pyroelectric phase transition of stuffed-tridymite-type BaZnGeO_4 . *Solid State Commun.* **2015**, *219*, 12–15, DOI 10.1016/j.ssc.2015.06.011.
16. George, S.; Anjana, P. S.; Deepu, V. N.; Mohanan, P.; Sebastian, M. T. Low-temperature sintering and microwave dielectric properties of $\text{Li}_2\text{MgSiO}_4$ ceramics. *J. Am. Ceram. Soc.* **2009**, *92*, 1244–1249, DOI 10.1111/j.1551-2916.2009.02998.x.
17. Wu, S. P.; Ma, Q. Synthesis, characterization and microwave dielectric properties of Zn_2GeO_4 ceramics. *J. Alloys Compd.* **2013**, *567*, 40–46, DOI 10.1016/j.jallcom.2013.03.052.
18. Chen, C. X.; Wu, S. P.; Fan, Y. X. Synthesis and microwave dielectric properties of B_2O_3 -doped Mg_2GeO_4 ceramics. *J. Alloys Compd.* **2013**, *578*,

- 153–156, DOI 10.1016/j.jallcom.2013.05.038.
19. Duijn, J. van; Graaff, R. A. G. de; Ijdo, D. J. W. Structure determination of CaMgGeO_4 . *Mater. Res. Bull.* **1995**, *30*, 1489–1493, DOI 10.1016/0025-5408(95)00158-1.
20. Xiang, H. C.; Fang, L.; Jiang, X. W.; Li, C.C. Low-firing and microwave dielectric properties of $\text{Na}_2\text{YMg}_2\text{V}_3\text{O}_{12}$ ceramic. *Ceram. Int.* **2016**, *42*, 3701–3705, DOI 10.1016/j.ceramint.2015.10.163.
21. Huang, C. L.; Huang, S. H. Low-loss microwave dielectric ceramics in the $(\text{Co}_{1-x}\text{Zn}_x)\text{TiO}_3$ ($x = 0-0.1$) system. *J. Alloys Compd.* **2012**, *515*, 8–11, DOI 10.1016/j.jallcom.2011.11.083.
22. Shannon, R. D. Dielectric polarizabilities of ions in oxides and fluorides. *J. Appl. Phys.* **1993**, *73*, 348–366, DOI 10.1063/1.353856.
23. Yoon, S. H.; Kim, D. W.; Cho, S. Y.; Hong, K. S. Investigation of the relations between structure and microwave dielectric properties of divalent metal tungstate compounds. *J. Eur. Ceram. Soc.* **2006**, *26*, 2051–2054, DOI 10.1016/j.jeurceramsoc.2005.09.058.
24. Zhou, D.; Randall, C. A.; Pang, L. X.; Wang, H.; Guo, J.; Zhang, G. Q.; Wu, X. G.; Shui, L.; Yao, X. Microwave dielectric properties of Li_2WO_4 ceramic with ultra-low sintering temperature. *J. Am. Ceram. Soc.* **2011**, *94*, 348–350, DOI 10.1111/j.1551-2916.2010.04312.x.

25. Yoon, S. H.; Choi, G. K.; Kim, D. W.; Cho, S. Y.; Hong, K.S. Mixture behavior and microwave dielectric properties of $(1-x)\text{CaWO}_4-x\text{TiO}_4$. *J. Eur. Ceram. Soc.* **2007**, *27*, 3087–3091, DOI 10.1016/j.jeurceramsoc.2006.11.035.
26. Fang, Z. X.; Tang, B.; Si, F.; Li, E. Z.; Yang, H. Y.; Zhang, S. R Phase evolution, structure and microwave dielectric properties of $\text{Li}_{2+x}\text{Mg}_3\text{SnO}_6$ ($x = 0.00\text{--}0.12$) ceramics. *Ceram. Int.* **2017**, *43*, 13645–13652, DOI 10.1016/j.ceramint.2017.07.074.
27. Kim, E. S.; Chun, B. S.; Freer, R.; Cernik, R. J. Effects of packing fraction and bond valence on microwave dielectric properties of $\text{A}^{2+}\text{B}^{6+}\text{O}_4$ (A^{2+} : Ca, Pb, Ba; B^{6+} : Mo, W) ceramics. *J. Eur. Ceram. Soc.* **2010**, *30*, 1731–1736, DOI 10.1016/j.jeurceramsoc.2009.12.018.
28. Chiang, C. C.; Wang, S. F.; Wang, Y. R.; Wei, W. C. J. Densification and microwave dielectric properties of $\text{CaO-B}_2\text{O}_3\text{-SiO}_2$ system glass-ceramics. *Ceram. Int.* **2008**, *34*, 599–604, DOI 10.1016/j.ceramint.2006.12.008.
29. Zhou, D.; Randall, C. A.; Wang, H.; Pang, L. X.; Yao, X. Microwave dielectric properties trends in a solid solution $(\text{Bi}_{1-x}\text{Ln}_x)_2\text{Mo}_2\text{O}_9$ ($\text{Ln} = \text{La}, \text{Nd}$, $0.0 \leq x \leq 0.2$) system. *J. Am. Ceram. Soc.* **2009**, *92*, 2931–2936, DOI 10.1111/j.1551-2916.2009.03307.x.
30. Colla, E. L.; Reaney, I. M.; Setter, N. Effect of structural changes in complex perovskites on the temperature coefficient of the relative permittivity. *J. Appl. Phys.* **1993**, *74*, 3414–3425, DOI 10.1063/1.354569.

31. Bosman, A. J.; Havinga, E. E. Temperature dependence of dielectric constants of cubic ionic compounds. *Phys. Rev.* **1963**, 129, 1593–1600, DOI 10.1103/PhysRev.129.1593.
32. Kweon, S. H.; Joung, M. R.; Kim, J. S.; Kim, B. Y.; Nahm, S.; Paik, J. H.; Kim, Y. S.; Sung, T. Y. Low temperature sintering and microwave dielectric properties of B₂O₃-added LiAlSiO₄ ceramic. *J. Am. Ceram. Soc.* **2011**, 94, 1995–1998, DOI 10.1111/j.1551-2916.2011.04619.x.
33. Varghese¹, J.; Vahera¹, T.; Ohsato, H.; Iwata, M.; Jantunen, H. Novel low-temperature sintering ceramic substrate based on indialite/cordierite glass ceramics. *Jpn. J. Appl. Phys.* **2017**, 56, 10PE01, DOI 10.7567/JJAP.56.10PE01.
34. Li, L. X.; Sun, H.; Cai, H.C. Microstructure and microwave dielectric characteristics of ZnZrNb₂O₈ and (Zn_{0.95}M_{0.05})ZrNb₂O₈ (M = Ni, Mg, Co and Mn) ceramics. *J. Alloy. Compd.* **2015**, 639, 516–519, DOI 10.1016/j.jallcom.2015.03.001.
35. Zhang, Y.; Liu, S.; Zhang, Y.; Xiang, M. Microwave dielectric properties of low-fired CoNb₂O₆ ceramics with B₂O₃ addition. *J. Mater. Sci: Mater. Electron.* **2016**, 27, 11293–11298, DOI 10.1007/s10854-016-5252-4.
36. Guo, Y.; Ohsato, H.; Kakimoto, K. I. Characterization and dielectric behavior of willemite and TiO₂-doped willemite ceramics at millimeter-wave frequency. *J. Eur. Ceram. Soc.* **2006**, 26, 1827–1830, DOI

- 10.1016/j.jeurceramsoc.2005.09.008.
37. Tsunooka, T.; Sugiyama, H.; Kakimoto, K.; Ohsato, H.; Ogawa, H. Zero temperature coefficient τ_f and sinterability of forsterite ceramics by rutile addition. *J. Ceram. Soc. Jpn.* **2004**, *112*, S1637–S1640, DOI 10.14852/jcersjsupl.112.0.S1637.0.
38. Ohsato, H.; Terada, M.; Kawamura, K. Fabrication conditions of diopside for millimeterwave dielectrics. *Jpn. J. Appl. Phys.* **2012**, *51* (9), 09LF02, DOI 10.1143/JJAP.51.09LF02.
39. Lei, W.; Lu, W. Z.; Liu, D.; Zhu, J. H. Phase evolution and microwave dielectric properties of $(1-x)\text{ZnAl}_2\text{O}_4\text{-}x\text{Mg}_2\text{TiO}_4$ ceramics. *J. Am. Ceram. Soc.* **2009**, *92* (1), 105–109, DOI 10.1111/j.1551-2916.2008.02757.x.
40. Fu, Z.; Liu, P.; Ma, J.; Zhao, X.; Zhang, H. Novel series of ultra-low loss microwave dielectric ceramics: $\text{Li}_2\text{Mg}_3\text{BO}_6$ (B = Ti, Sn, Zr). *J. Eur. Ceram. Soc.* **2016**, *36* (3), 625–629, DOI 10.1016/j.jeurceramsoc.2015.10.040.
41. Xiang, H. C.; Li, C. C.; Yin, C. Z.; Tang, Y.; Fang, L. A reduced sintering temperature and improvement in the microwave dielectric properties of $\text{Li}_2\text{Mg}_3\text{TiO}_6$ through Ge substitution. *Ceram. Int.* **2018**, *44*, 5817–5821, DOI 10.1016/j.ceramint.2017.12.167.
42. Bi, J. X.; Li, C. C.; Zhang, Y. H.; Xing, C. F.; Yang, C. H.; Wu, H. T. Crystal structure, infrared spectra and microwave dielectric properties of ultra low-loss $\text{Li}_2\text{Mg}_4\text{TiO}_7$ ceramics. *Mater. Lett.* **2017**, *196*, 128–131, DOI

1
2
3 10.1016/j.matlet.2017.03.038.
4
5

6
7 43. Bi, J. X.; Niu, Y. J.; Wu, H. T. $\text{Li}_4\text{Mg}_3\text{Ti}_2\text{O}_9$: A novel low-loss microwave
8
9 dielectric ceramic for LTCC applications. *Ceram. Int.* **2017**, *43*, 7522–7530,
10
11 DOI 10.1016/j.ceramint.2017.03.041.
12

13
14 44. Pan, H. L.; Wu, H. T. Crystal structure, infrared spectra and microwave
15
16 dielectric properties of new ultra low-loss $\text{Li}_6\text{Mg}_7\text{Ti}_3\text{O}_{16}$ ceramics. *Ceram. Int.*
17
18 **2017**, *43*, 14484–14487, DOI 10.1016/j.ceramint.2017.06.184.
19
20

21
22 45. Matsumoto, H.; Tamura, H.; Wakino, K. $\text{Ba}(\text{MgTa})\text{O}_3$ - BaSnO_3 high Q
23
24 dielectric resonator. *Jpn. J. Appl. Phys.* **1991**, *30*, 2347–2349, DOI
25
26 10.1143/JJAP.30.2347.
27
28

29
30 46. Kawashima, S.; Nishida, M.; Ueda, I.; Ouchi, H. $\text{Ba}(\text{Zn}_{1/3}\text{Ta}_{2/3})\text{O}_3$ ceramics
31
32 with low dielectric loss at microwave frequencies. *J. Am. Ceram. Soc.* **1983**,
33
34 *66*, 421–423, DOI 10.1111/j.1151-2916.1983.tb10074.x.
35
36
37
38
39
40
41
42
43
44
45
46
47
48
49
50
51
52
53
54
55
56
57
58
59
60

Table I The atomic coordinates of CaMgGeO₄ and the reliability factors

Ceramic	Atom	Site	x/a	y/b	z/c	Biso.	Occ.
CaMgGeO ₄	Ca	4c	0.2242(2)	1/4	0.03624(3)	0.4334(7)	0.5
	Mg	4a	0	0	0	0.4896(7)	0.5
	Ge	4c	0.4197(7)	1/4	0.07875(1)	0.2272(8)	0.5
	O(1)	8d	0.34969(2)	1/4	0.23099(4)	0.1731(3)	1
	O(2)	4c	0.05856(4)	1/4	0.23220(6)	1.1751(8)	0.5
	O(3)	4c	0.41093(3)	1/4	0.72671(5)	1.4031(7)	0.5

Table II Sintering temperature, density and microwave dielectric properties of CaMgGeO₄ + 5wt% B₂O₃ ceramics sintered at different temperatures.

Composition	S.T. (°C)	ρ (g/cm ³)	ϵ_r	$Q \times f$ (GHz)	τ_f (ppm/°C)
CaMgGeO ₄	1300	3.57	6.71	124,900	-73.7
	900	3.55	5.21	82,600	-68.6
	920	3.59	5.43	95,600	-67.0
CaMgGeO ₄ +5wt% B ₂ O ₃	940	3.62	5.80	102,000	-64.7
	960	3.62	5.56	85,210	-66.5
	980	3.60	5.23	70,880	-64.9

Table III Ultra-low loss dielectric ceramics and their properties

Ceramics	S.T. (°C)	Crystal Structure	ϵ_r	$Q \times f$ (GHz)	τ_f (ppm/°C)	Reference
CaMgGeO ₄	1300/6h	Orthorhombic <i>Pbmn</i> Olivine	6.71	124,900	-73.7	This work

CaMgGeO ₄ +5wt% B ₂ O ₃	940/6h	Orthorhombic <i>Pbmn</i> Olivine	5.80	102,000	-64.7	This work
Zn ₂ GeO ₄	1300/4h	Rhombohedral <i>R-3</i>	6.87	102,700	-32.4	[17]
Mg ₂ GeO ₄ +3wt% B ₂ O ₃	1250/4h	Orthorhombic <i>Pbmn</i> Olivine	6.76	95,000	-28.7	[18]
Zn ₂ SiO ₄	1320/CIP	Rhombohedral <i>R-3</i> Willemite	6.6	219,000	-61	[36]
Mg ₂ SiO ₄	1450/2h	Forsterite	6.8	270,000	-67	[37]
CaMgSi ₂ O ₆	1300/CIP	Monoclinic C12/c1	7.6	121,380	-66	[38]
Mg ₂ TiO ₄	1450/4h	Cubic <i>Fd-3m</i> Spinel	14	150,000	-50	[39]
Li ₂ Mg ₃ TiO ₆	1280/6h	Cubic <i>Fd-3m</i> Rock-salt	15.2	152,000	-39	[40]
Li ₂ Mg ₃ Ti _{0.9} Ge _{0.1} O ₆	1140/6h	Cubic <i>Fd-3m</i> Rock-salt	13.7	131,500	-34.2	[41]
Li ₂ Mg ₄ TiO ₇	1600/4h	Cubic <i>Fd-3m</i> Rock-salt	13.43	233,600	-7.24	[42]
Li ₄ Mg ₃ Ti ₂ O ₉	1450/4h	Cubic <i>Fd-3m</i> Rock-salt	15.97	135,800	-7.06	[43]
Li ₆ Mg ₇ Ti ₃ O ₁₆	1550/4h	Cubic <i>Fd-3m</i> Rock-salt	15.27	209,400	-11.32	[44]
Ba(Mg _{1/3} Ta _{2/3})O ₃	1640/100h	Complex perovskite	24	430,000	8	[45]
Ba(Zn _{1/3} Ta _{2/3})O ₃	1350/120h	Complex perovskite	28	168,000	1	[46]

FIGURE CAPTIONS:

Figure 1 X-ray diffraction pattern of CaMgGeO_4 calcined at 1250 °C (a), Rietveld refinement of the room temperature XRD data and schematic crystal structure for CaMgGeO_4 (b).

Figure 2 Raman spectrum of CaMgGeO_4 in the range of 60-1050 cm^{-1} .

Figure 3 Microstructures of CaMgGeO_4 ceramics sintered at 1260 °C (a), 1280 °C (b), 1300 °C (c), 1320 °C (d), 1340 °C (e).

Figure 4 The ϵ_r , $Q \times f$ and τ_f values of CaMgGeO_4 ceramics as a function of temperature.

Figure 5 Thermal expansion curve in the temperature range of 25-900 °C of CaMgGeO_4 sintered at 1300 °C.

Figure 6 The temperature dependence of relative permittivity (ϵ_r) and loss tangent ($\tan \delta$) at four different frequencies (1 kHz, 10 kHz, 100 kHz, and 1 MHz).

Figure 7 The bulk densities of CaMgGeO_4 ceramic with different B_2O_3 contents as a function of sintering temperature.

Figure 8 XRD patterns of CaMgGeO_4 ceramic with different B_2O_3 additions sintered at densification temperatures.

Figure 9 XRD pattern, BSE image and EDS analysis of $\text{CaMgGeO}_4 + 5\text{wt}\% \text{B}_2\text{O}_3 + 20\text{wt}\% \text{Ag}$ samples co-fired at 940 °C for 6h.

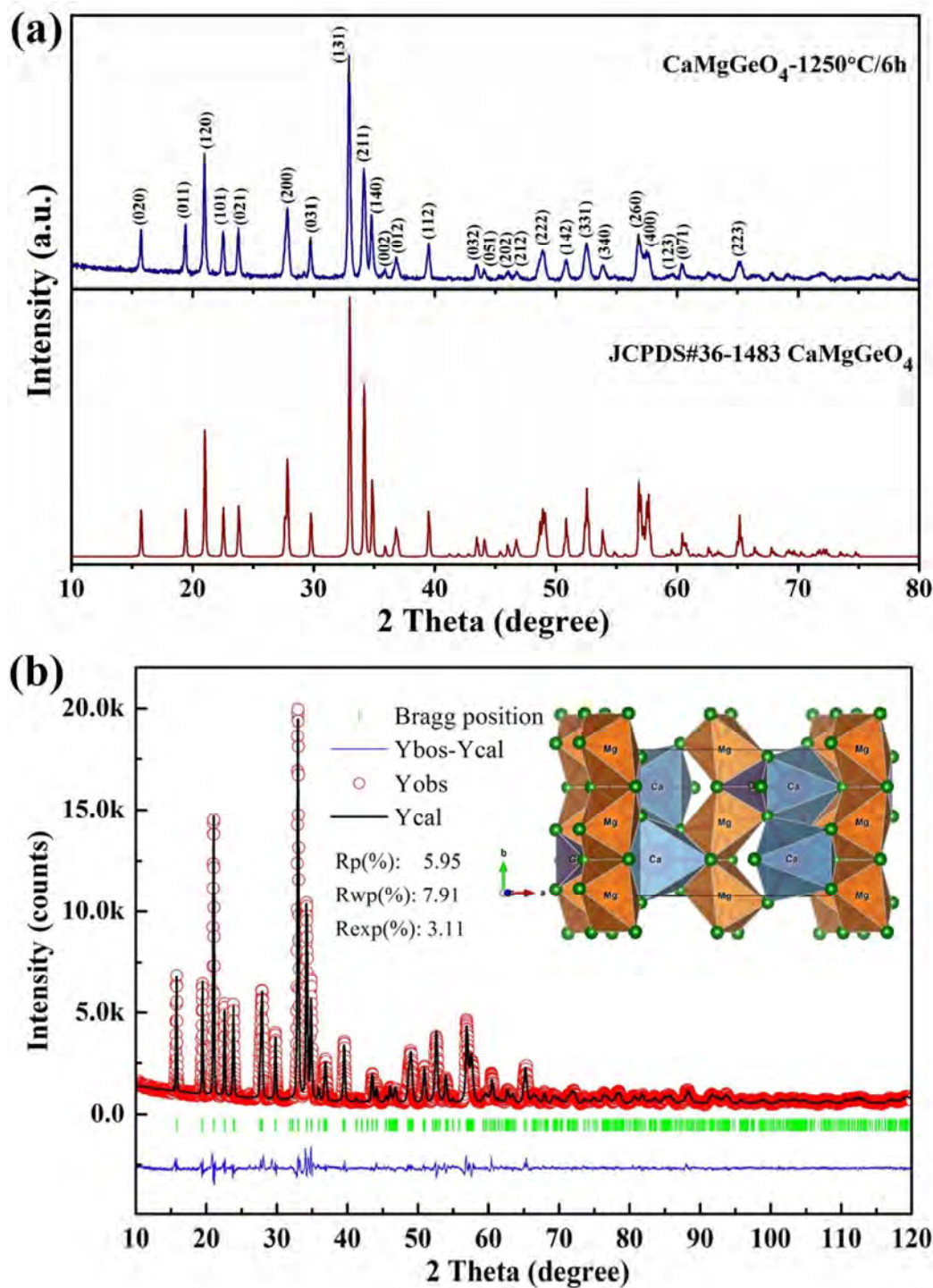


Figure 1

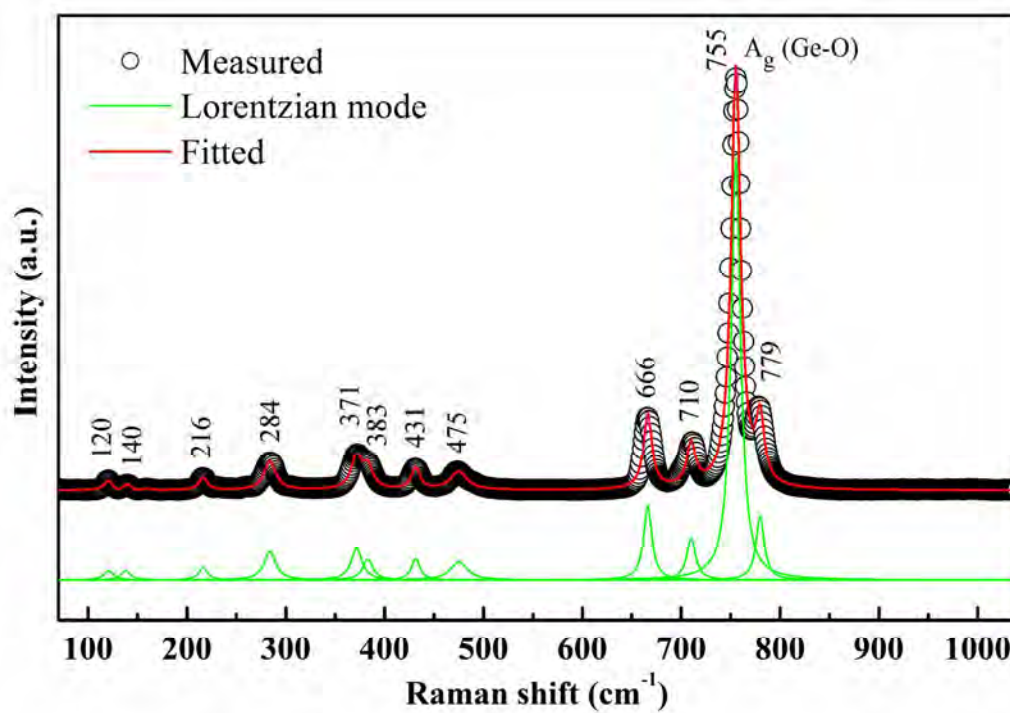


Figure 2

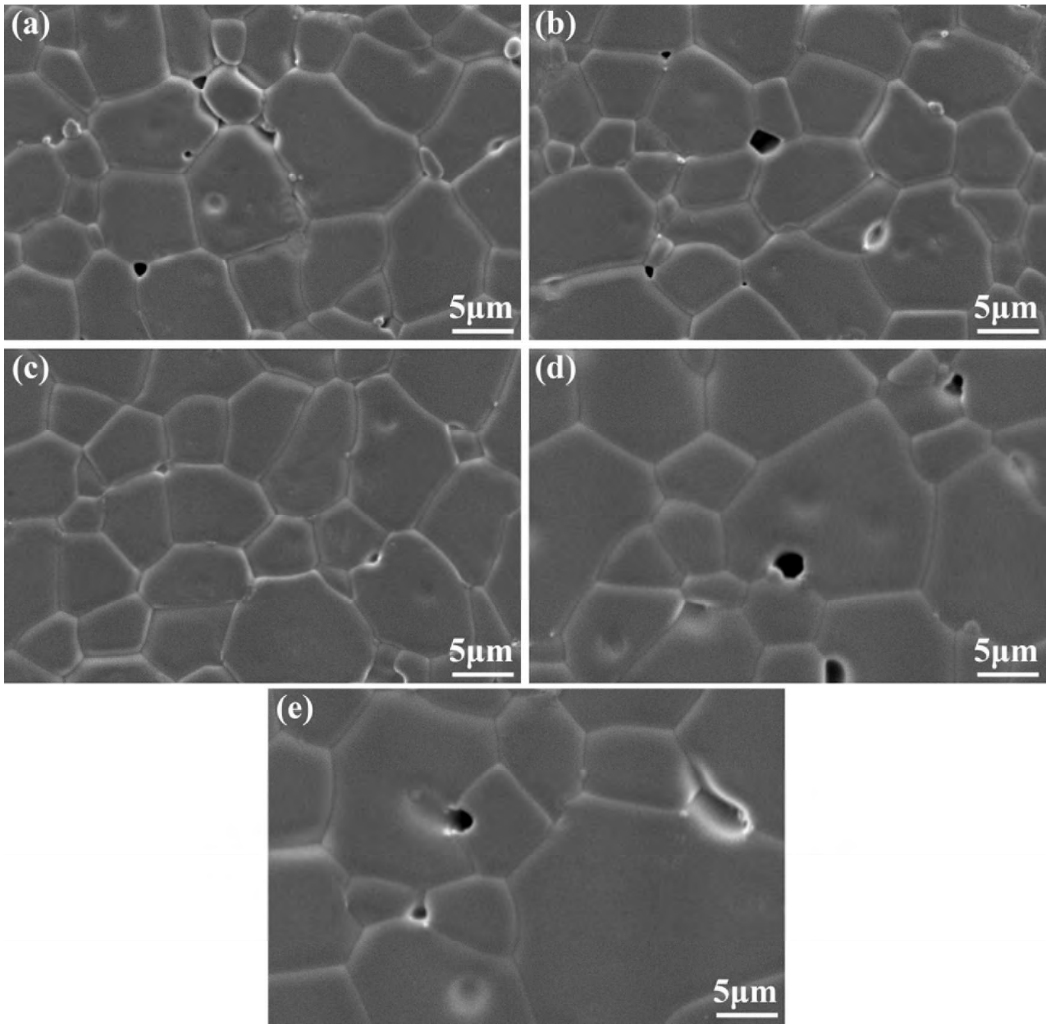


Figure 3

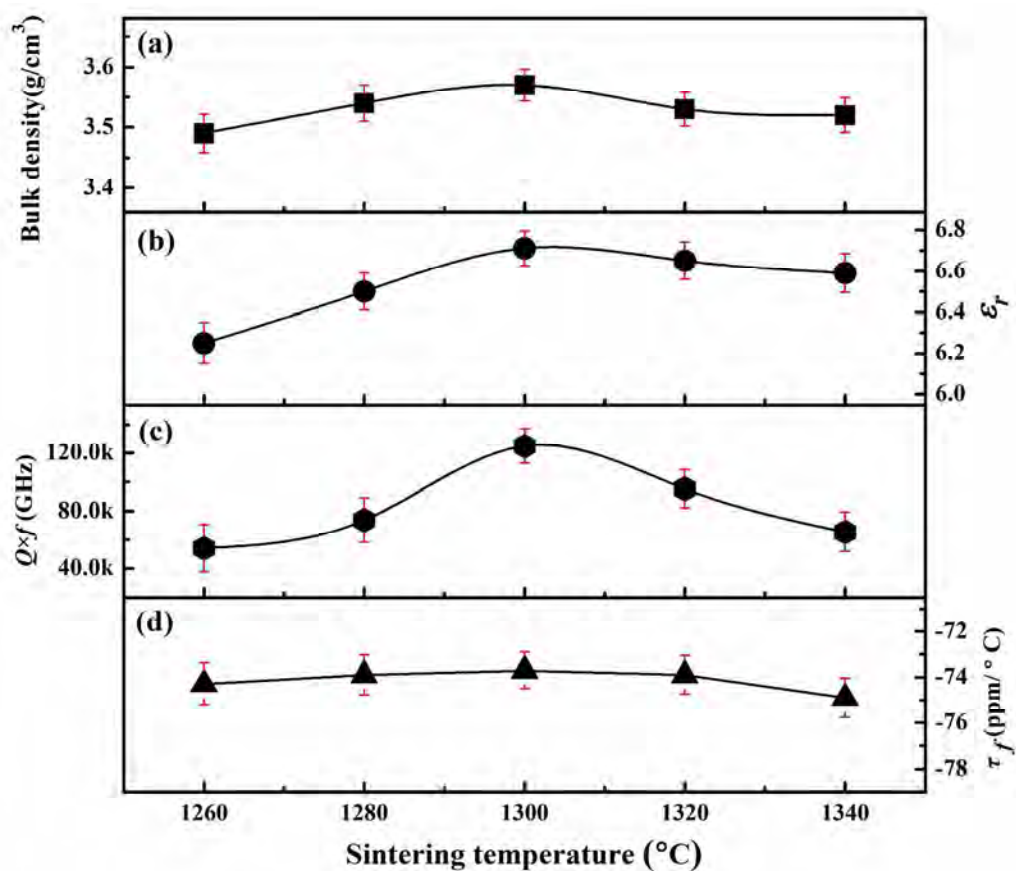


Figure 4

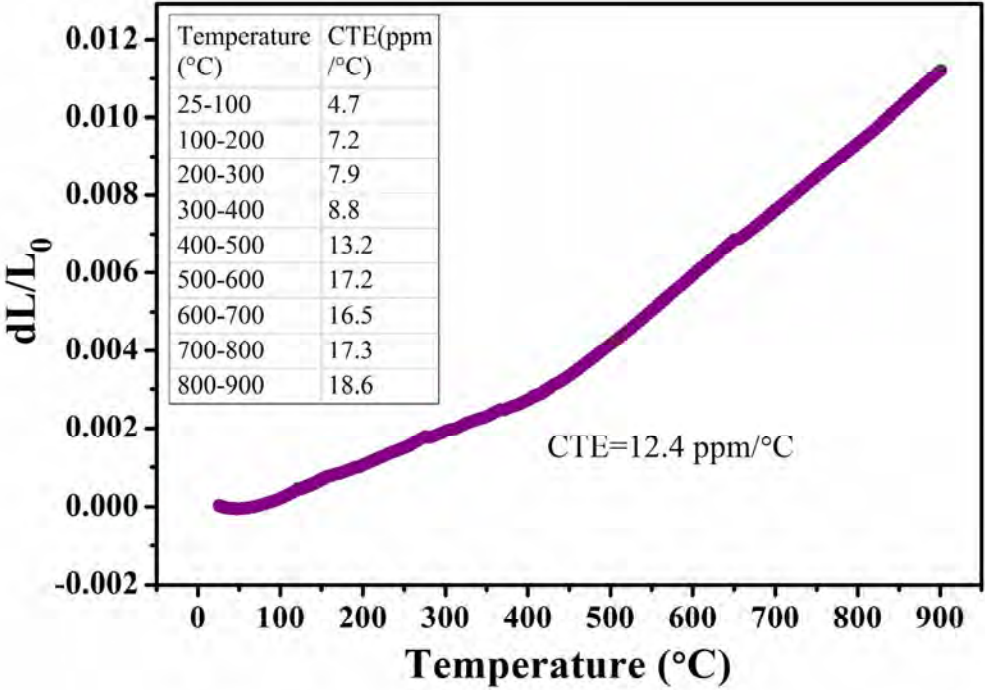


Figure 5

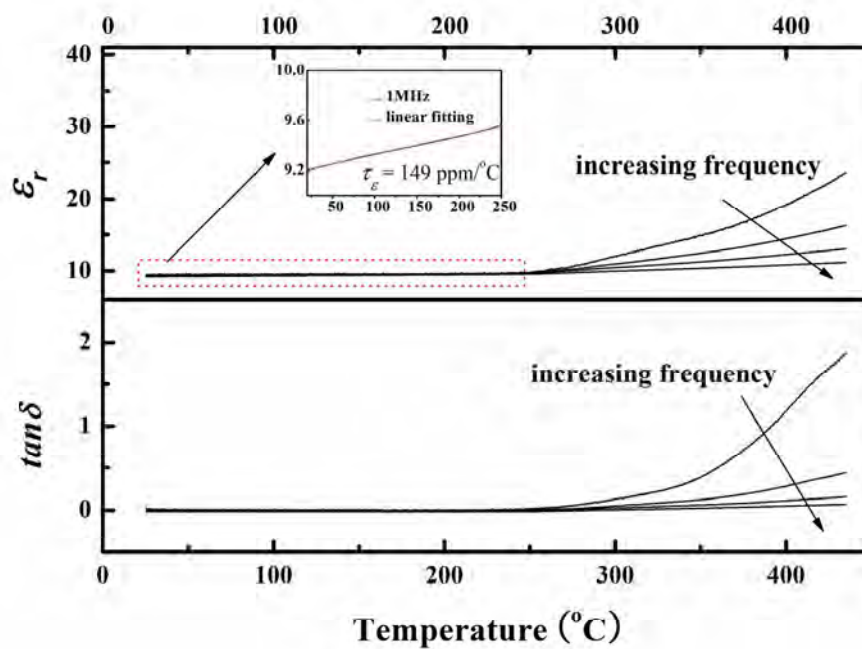


Figure 6

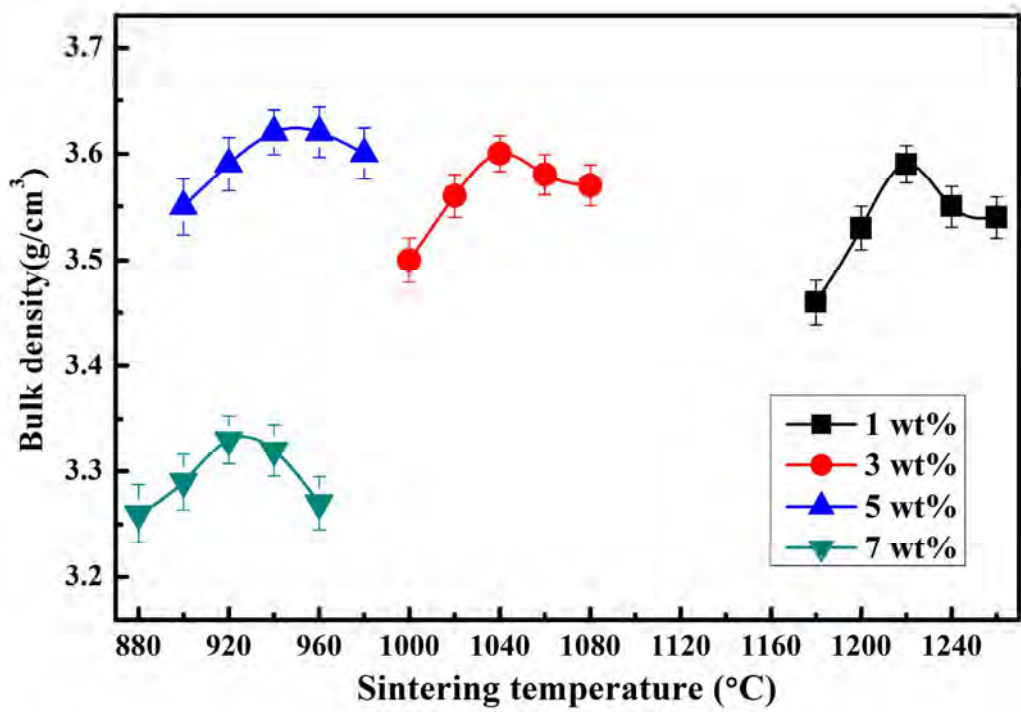


Figure 7

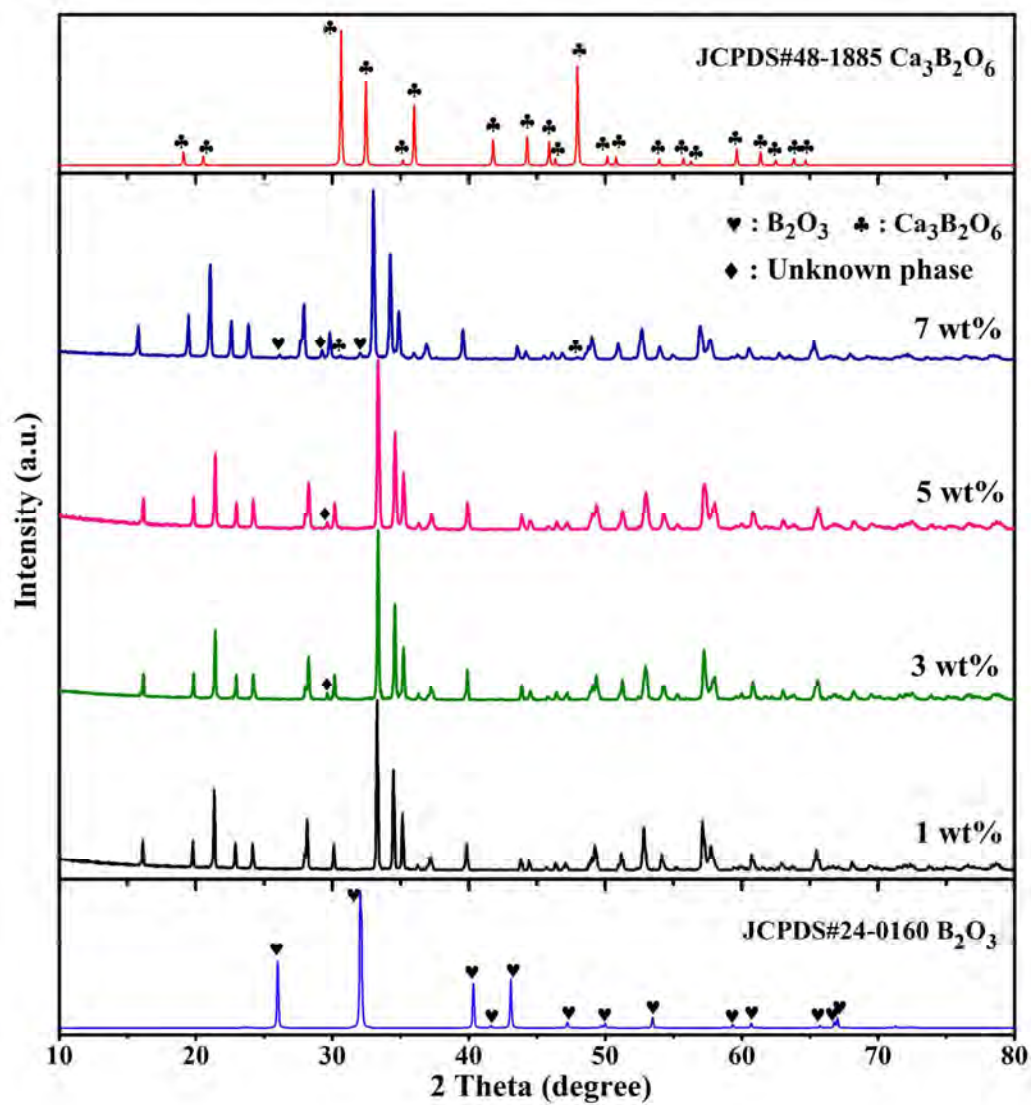


Figure 8

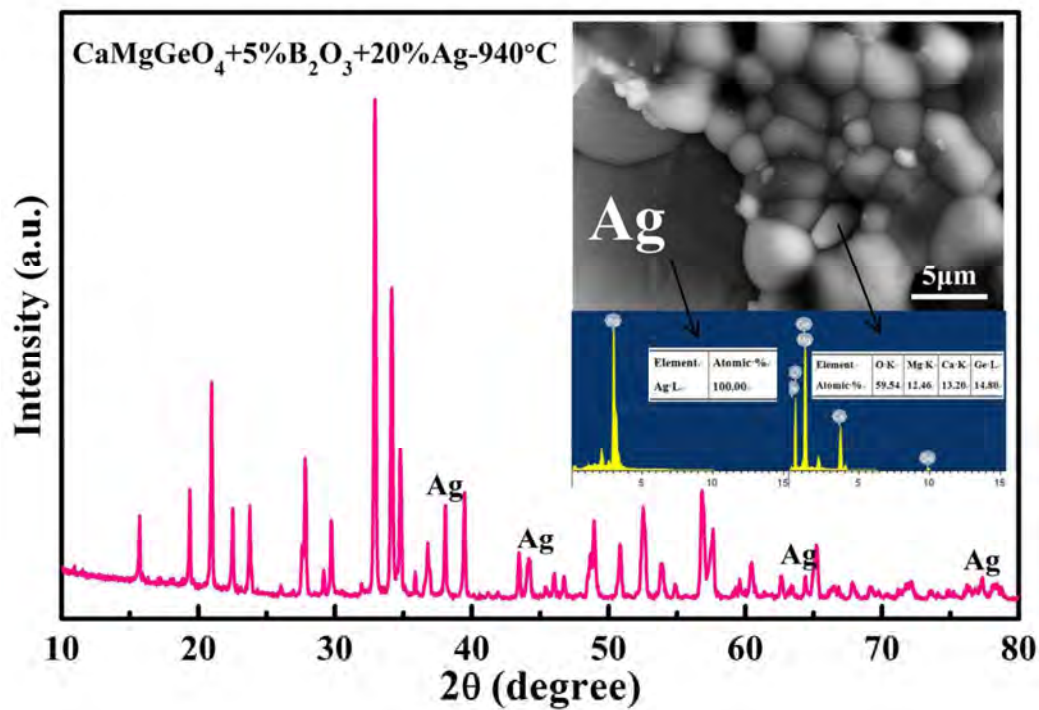
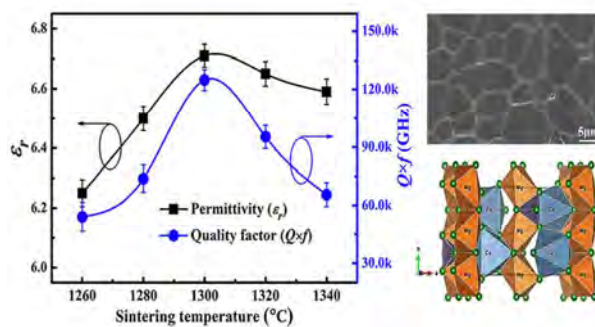


Figure 9

For Table of Contents Use Only



Synopsis

Low permittivity and ultra-low dielectric loss make the olivine structural CaMgGeO₄-based ceramics suitable candidate for substrates and packaging applications.